

OMAE2003-37472

RELIABILITY REASSESSMENT OF A JACKET PLATFORM WITH GAS SEEPAGE IN THE SOUTH CHINA SEA

Gudfinnur Sigurdsson
Det Norske Veritas
N-1322 Høvik, Norway
Email: Gudfinnur.Sigurdsson@dnv.com

Jan Mathisen
Det Norske Veritas
N-1322 Høvik, Norway
Email: Jan.Mathisen@dnv.com

Pål Strøm
Det Norske Veritas
N-1322 Høvik, Norway
Email: Pal.Strom@dnv.com

Tok Kwong Goh
Petronas Research & Scientific Services
Kajang, Selangor, Malaysia
Email: gohtk@petronas.com.my

ABSTRACT

A structural reliability analysis is carried out on a jacket platform in 75 m water depth, in the South China Sea. A platform collapse failure mode is considered, with emphasis on uncertain soil conditions around the pile foundations, due to gas seepage while the platform has been in service. Random environmental conditions due to wind, waves and current are taken into account, based on observed data. Allowance for the short duration of environmental measurements is included and has a marked effect on the results. Two response surfaces are applied in the reliability calculation, to model the loads and the system capacity.

INTRODUCTION

A reliability analysis was carried out for an ageing platform located in the South China Sea, in 75m water depth. This is a conventional 8-legged steel jacket structure (Figure 1). It has been in operation since 1983.

Installation of a new gas compression module on this platform has been proposed. This will impose additional loads on the platform and foundation. Further, there is somewhat increased uncertainty in the soil properties around the platform foundation, due to gas seepage from the reservoir.

Preliminary pushover analysis indicated that the critical failure mode occurred during the North-East Monsoon condition. The dominant failure mode involved lateral failure of the soil around the upper parts of the piles, bending of the piles, and global horizontal displacement of the jacket structure.

The focus of the reliability analysis is to study the shallow gas impact on the jacket structure. The results of the analysis are presented in the following sections.

NOMENCLATURE

g	limit state function
H_R, h	individual wave height
H_S, h_S	significant wave height
L, l	applied base shear force
l_C	characteristic base shear force
OCR	over-consolidation ratio
S_U, s_U	static undrained shear strength
T	wave period
U_C	model uncertainty factor on capacity
U_L	model uncertainty factor on applied load
U_{cy}, u_{cy}	cyclic loading factor
V, v	mean wind speed
X_{pp}, x_{pp}	excess pore pressure
A, α	slope parameter of Weibull dstn. of H_S
B, β	shape parameter of Weibull dstn. of H_S
ε_{50}	strain leading to mobilization of 50% of strength
λ	capacity factor w.r.t. characteristic base shear force
τ_S	short term duration
τ_L	long term duration
σ_{v0}'	effective vertical in-situ stress
Ψ, ψ	vector of environmental conditions
ζ	height of line of action of applied force above mudline



Figure 1 Finite element model of jacket structure.

PROBABILISTIC FORMULATION

Failure Mode

The dominant failure mode is illustrated in Figure 2. It occurs when horizontal loads on the jacket lead to deflection of the upper parts of the piles combined with yielding of the soil in this region. Plastic hinges develop in the piles and the jacket, itself, moves horizontally.

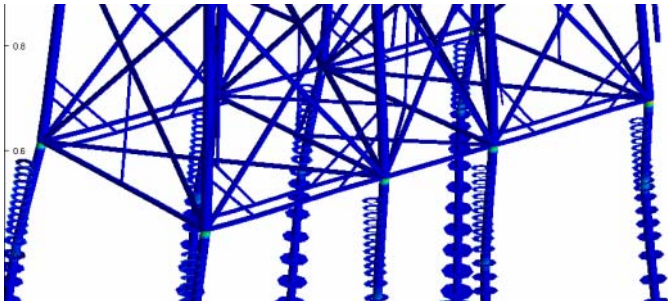


Figure 2 Bottom part of jacket and upper part of piles, showing dominant failure mode.

Extensive, deterministic, collapse analyses and sensitivity studies lead to the assumption that contributions from other modes of failure are negligible in the present case. This situation is naturally related to the relatively low shear strength in the upper regions of the soil, and to the gas seepage that has occurred.

Definition of Capacity

The collapse analyses are carried out with the USFOS program, ref.[1]. In these analyses, the environmental loading is gradually incremented by a load factor, and the structural response is computed at each load step, as indicated in Figure 3. The precise failure situation is defined by the peak of the curve; i.e. the capacity corresponds to the maximum load that the structure and foundation can resist.

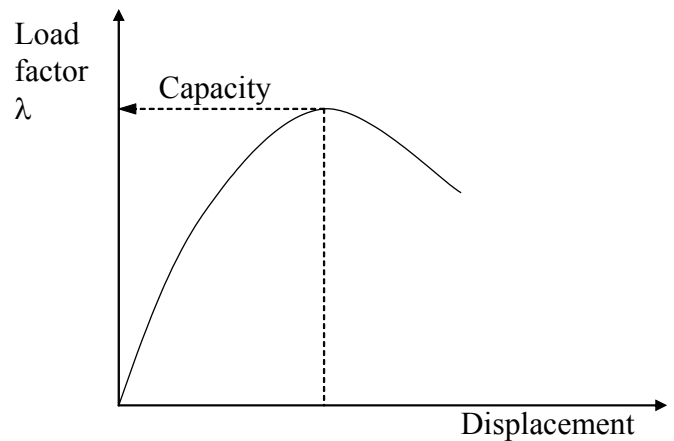


Figure 3 Definition of capacity.

In general, this form of capacity is a function of the direction of the loads with respect to the platform orientation and the overall distribution of the loads on the platform, as well as the material properties and design of the jacket. With the present mode of lateral failure near the mudline, the load distribution can conveniently be parameterized in terms of the magnitude of the base shear force l and the height of the line of action of this force ζ . The capacity factor λ is normalised with respect to the characteristic value of base shear force computed for deterministic design analysis l_c .

Limit state function

Hence, the basic form of the limit state function can be written as the difference between the capacity for base shear force and the applied base shear force

$$g = \lambda(\zeta) \cdot l_c - l \quad (1)$$

where the notation emphasizes that capacity factor λ is a function of the height of the applied load ζ . It is understood that both loads and capacity are dependent on the direction of the environmental effects approaching the platform. However, a single main direction is considered at a time and we choose not to explicitly show this dependency in the limit state function. The applied load and the height of the load is dependent on the wind, wave and current conditions, which are

collected in the random vector Ψ , and this dependency is included by rewriting the limit state function as

$$g = \lambda[\zeta(\psi)] \cdot l_c - l(\psi) \quad (2)$$

Model uncertainty factors on capacity U_C and load U_L are also introduced into the limit state function to give

$$g = u_c \cdot \lambda[\zeta(\psi)] \cdot l_c - u_L \cdot l(\psi) \quad (3)$$

This expression is converted to a smoother, logarithmic form to assist the numerical optimization in the actual reliability computation. Figure 4 shows an overview of the data flow through the reliability analysis. The input random variables are described next, followed by the load and capacity modules.

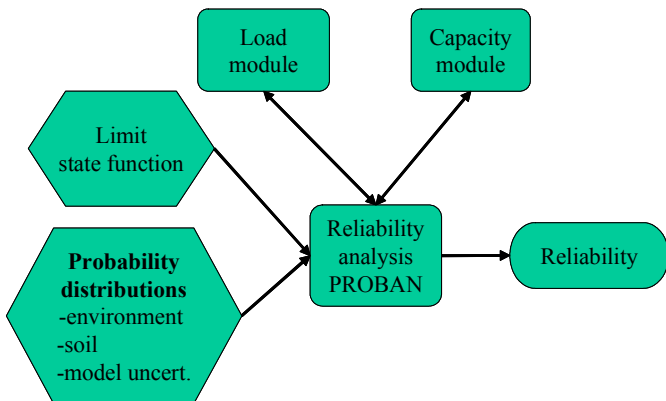


Figure 4 Overview of reliability analysis.

ENVIRONMENTAL VARIABLES

Both 1¼ years of measured environmental data and 20 years of hindcast environmental data were available for the platform site. However, a decision was made to base the analysis primarily on the measured data due to some weakness in these particular hindcast data.

Wave directions

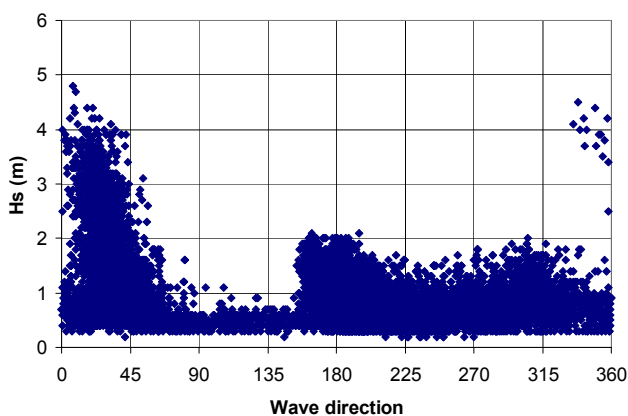


Figure 5 Scatter plot of significant wave height against direction waves are coming from, from measured data.

It is clear that the most severe waves approach from 0° to 45° ; i.e. from the N to NE, from Figure 5. Deterministic

collapse analyses with characteristic wave heights for the various directions confirmed that waves from the NE would dominate the probability of failure. Hence, the reliability analysis could be limited to this sector, assuming that the contributions to the probability of failure from the other directions are negligible in comparison. The probability of occurrence of waves in this sector is found to be 45% from the hindcast data. The mean zero-up-crossing period of waves in this sector is found to be 5.3s. Hence, the number of individual waves from this sector during one year is approximately 2.7×10^6 .

Long term distribution of significant wave height

The measured wave data is filtered to include exactly one year of data, from measurements every 3 hours, and only waves approaching from the compass sector from 0° to 45° . A Weibull distribution is fitted to these data. The cumulative distribution function may be written as:

$$F_{H_s}(h_s; \alpha, \beta, \gamma) = 1 - \exp\left\{-\left(\frac{h_s - \gamma}{\alpha}\right)^\beta\right\} \quad (4)$$

where the fitted parameters are:

scale parameter $\alpha = 1.36$ m,

shape parameter $\beta = 1.64$,

threshold parameter $\gamma = 0.39$ m.

It is unsatisfactory to base a long term distribution of wave height on only a single year's data. Annual and longer term variation is missed. This can be rectified with the help of uncertainty modelling from the hindcast data.

The hindcast data is split into groups of annual data. Wave data from the NE direction are selected, and Weibull distributions are fitted to the data for each year. The fitted parameters are shown in Figure 6. The variation in the parameters from year to year is considerable. Note that the threshold parameter has been limited to 0.5 m at most, for practical reasons in the fitting process. This parameter has a relatively smaller effect on the distribution than the other two parameters, and its variability is not included in the uncertainty modelling.

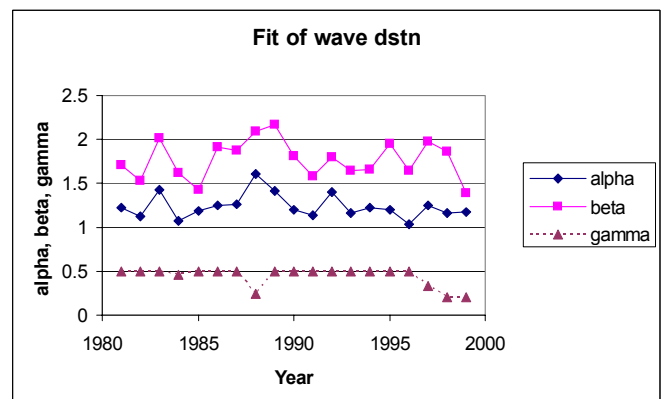


Figure 6 Variation of parameters of Weibull distribution fitted to hindcast, annual data for significant wave heights.

The variability may be summarised in terms of the coefficients of variation and correlation coefficient:

coefficient of variation for scale parameter = 0.11

coefficient of variation for shape parameter = 0.12

correlation coefficient between scale and shape parameters = 0.69

This data is used to define a bivariate, normal, density function for the parameters of the Weibull distribution in equation (4), denoted by $f_{A,B}(\alpha, \beta)$.

Annual Extreme Value distribution of Individual Wave Height

A variation on the Rayleigh distribution from Næss (ref.[2]) is adopted to describe the short term distribution of individual wave heights, conditional on the significant wave height. This formulation takes account of the effect of the bandwidth of the wave spectrum on the correlation between adjacent wave crests and troughs. The distribution is written as

$$F_{H_R|H_S}(h|h_S) = 1 - \exp\left\{-\frac{h^2}{h_S^2(1-r(T/2))/4}\right\} \quad (5)$$

where $r(T/2)$ is the value of the autocorrelation function of the surface elevation, at a time lag of one half wave period, and normalised by the variance of the surface elevation. Næss indicates typical values of this parameter to lie in the range from 0.65 to 0.80 for some common wave spectra, and a value of 0.71 is assumed in the following. Note also, that the significant wave height is here assumed to be defined as 4 times the standard deviation of the surface elevation.

The short term extreme value distribution of the largest individual wave height may then be written as follows, when the wave heights are assumed independent

$$F_{H_R^*|H_S}(h|h_S; \tau_S) = [F_{H_R|H_S}(h|h_S)]^{N_S} \quad (6)$$

where $\tau_S = 10800$ s is the duration of the short term sea state, assumed equal to 3 hours, for consistency with the wave data for the significant wave height, and the number of waves in the short term state is calculated as $N_S = \tau_S / T_Z$. The subscript S on the duration indicates Short term.

The marginal, extreme value distribution of individual wave height in a single, random short term state is obtained by applying the theorem of total probability and integrating over the domain of significant wave heights and uncertain distribution parameters for significant wave height

$$F_{H_R^*}(h; \tau_S) = \int F_{H_R^*|H_S}(h|h_S; \tau_S) f_{H_S}(h_S; \alpha, \beta, \gamma) f_{A,B}(\alpha, \beta) dh_S d\alpha d\beta \quad (7)$$

where $f_{H_S}(h_S; \alpha, \beta, \gamma)$ is the Weibull, probability density of the significant wave height, corresponding to the cumulative distribution function in equation (4). This integration is carried out using a first order reliability method with the PROBAN program, ref.[3]. The annual extreme value distribution of individual wave height is then written as follows, when the short term states are assumed independent

$$F_{H_R^*}(h; \tau_L) = [F_{H_R^*}(h; \tau_S)]^{N_L} \quad (8)$$

where $\tau_L = 365.25 \times 24 \times 3600$ s is the duration of one year, and the number of sea states from the chosen sector in one year is calculated as $N_L = 0.455 \times \tau_L / \tau_S = 1330$. The subscript L indicates long term. A Gumbel distribution is fitted to the results for the annual extreme individual wave height.

Conditional distribution of Wind Speed

The joint probability density function of significant wave height and wind speed is denoted by

$$f_{H_S, V}(h, v) = f_{H_S}(h) \cdot f_{V|H_S}(v|h) \quad (9)$$

where $f_{H_S}(h)$ is the marginal, Weibull, probability density of the significant wave height, corresponding to the cumulative distribution function in equation (4), and $f_{V|H_S}(v|h)$ is the conditional probability density of the wind speed. A conditional Weibull distribution is applied for the wind speed distribution. The parameters of this distribution are made functions of the significant wave height, as described in ref.[4] Contour plots of the data and fitted distribution are shown in Figure 7 and Figure 8.

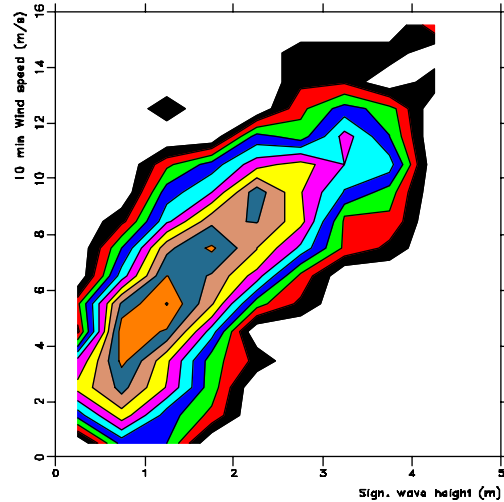


Figure 7 Logarithmic contour plot of measured data for significant wave height and 10 minute wind speed at 20 m above MSL.

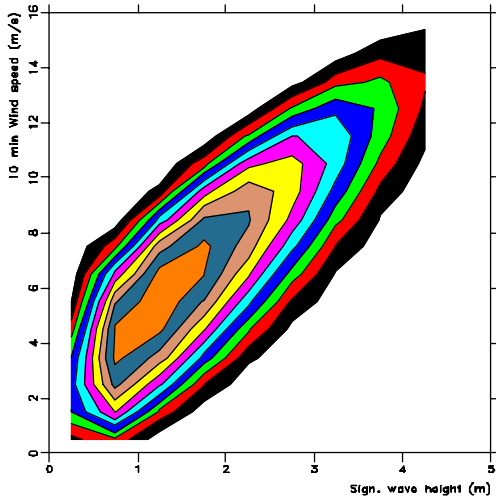


Figure 8 Logarithmic contour plot of fitted joint distribution for significant wave height and 10 minute wind speed at 20 m above MSL.

Other environmental variables

Relatively little information is available for current speeds. A Weibull distribution is fitted to the long term current data, and a correlation coefficient of 0.9 is assumed with the annual extreme wave height, in order to ensure a conservative dependency between these two variables.

A deterministic, low water level is assumed, because sensitivity studies show that the base shear force tends to increase with decreasing water level.

A regular wave period of 12 s is assumed. This is a reasonable value compared to the 100-year conditions for characteristic loads on the platform. Furthermore, sensitivity studies show the sensitivity to wave period is fairly low.

Marine growth is assumed to be equal to the extent applied in the platform design analysis. Again, sensitivity studies confirm that this assumption does not seriously affect the estimated reliability.

SOIL VARIABLES

Shear strength

Static undrained shear strength (s_u) is the primary soil variable. Data from the site indicated that the shear strength profile could be modeled with a seabed intercept and a linear increase in the shear strength with depth. There is some random local variation, but this tends to average out over the length of a long pile, with respect to the vertical capacity of the pile. Such averaging is not equally effective with respect to the lateral capacity of a pile, since this is dominated by the soil strength within the upper 10-20 metres or so.

Cyclic loading factor

The soil strength model is then corrected by a cyclic loading factor (U_{cy}). This factor accounts for the cyclic loading due to waves. The cyclic loading factor is a function of the

average shear stress, the number of load cycles, and the distribution of the shear stress amplitudes in the design storm.

Elasticity

The elastic characteristics of the soil are largely specified in terms of the strain leading to mobilisation of 50% of the soil strength (ε_{50}). This variable is based on laboratory tests of relevant soil types and includes some uncertainty

Excess pore pressure

Some gas seepage has occurred in the vicinity of the platform. The gas typically seeps up along a well casing until it encounters a permeable rock layer, where it diffuses outwards from the well and upwards into the soil above. Such gas causes an excess pressure (X_{pp}) in the pores of the clay surrounding the foundation piles. Data on the excess pore pressure is obtained from piezoprobe dissipation tests carried out in two boreholes in 1994 and two boreholes in 2001. The axial capacity of the piles is particularly sensitive to excess pore pressure, and the lateral capacity is also affected.

Spatial averaging

For evaluation of the overall stability of the foundation under extreme loading conditions, the spatially averaged soil strength properties over the extent of the foundation are of interest. Soil strength properties exhibit spatial connectivity vertically as well as laterally; i.e. there is correlation between the soil strengths from one point to another within the soil volume. The horizontal correlation length of the soil strength field is usually much larger than the vertical correlation length.

The axial capacities of the piles in the present foundation come about as the skin friction integrated over the respective pile lengths. For the axial capacities, it can therefore be assumed that the effects of the local fluctuations of the skin friction from point to point along each pile will average out over the length of the pile, and the axial capacities of all piles can thus be represented by capacities calculated from average skin friction properties only, without considering any local variability.

The lateral capacities of the piles come about from a much more localized soil strength, i.e. it arises from the soil strength in a limited zone near the soil surface. The vertical extent of this zone is so limited that for practical purposes it will not be reasonable to count on any effect of spatial averaging vertically. This leaves horizontal spatial averaging to be considered for its influence on the lateral capacities of the piles in the present foundation.

Table 1 Stochastic soil variables and their respective probabilistic models

Variable	Distribution type	Mean value	Standard deviation
S_u	Fixed	12.2+1.93z (kPa)	N/A for axial resistance
S_u	Normal	12.2+1.93z (kPa)	6.0 kPa *
U_{cy}	Normal	0.9	0.09
ε_{50}	Normal	1.15%	0.174% *
X_{pp} **	Normal	-33.2+2.22z (kPa)	50.4 kPa

* after reduction for spatial averaging w.r.t. lateral resistance

** cut-off limits: $X_{pp} \leq$ minor principal soil stress and $X_{pp} \geq 0$

The lateral pile capacity is approximately proportional to the undrained shear strength of the soil. It is also dependent on the strength and stiffness of the pile, but the uncertainty related to these quantities is relatively small. Hence, the spatial average of the lateral pile capacities over the lateral extent of the present foundation will therefore come about in the same manner as the spatial average of the undrained shear strength over this extent. In the structural reliability analysis, it will therefore suffice to represent the lateral capacity of each pile as the lateral capacity that comes about from a calculation on the basis of a spatially averaged undrained shear strength profile.

The effect of shallow gas seeping into soil increases the pore pressure in the layers of soil. This reduces the effective stresses in the soil with a subsequent reduction in shear strength. The reduction is dependent on the magnitude of excess pore pressure. In order to account for the excess pore pressure X_{pp} , we apply the following expression, based on the modified SHANSEP procedure ref.[8]:

$$\frac{s_u}{s_{u,NC}} = (OCR)^{0.2} = \left(\frac{\sigma_{v0}}{\sigma_{v0} - X_{pp}} \right)^{0.2} \quad (10)$$

When the confining stress situation decreases due to the excess pore pressure, the effect on the skin friction is assumed proportional to the effect on the shear strength, reflecting the fact that the piles are driven in (close to) normally consolidated clay, setting up the skin friction according to the α -method recommended by API.

An alternative to this procedure would be to model the input parameter ψ , in the α -method, with direct allowance for the reduced confining pressure. However, the sensitivity to using such an alternative formulation is expected to be relatively small.

MODEL UNCERTAINTY

Two model uncertainties are applied as multiplicative factors, as indicated in (3). The model uncertainty on the load is taken as a normal variable with a mean value of 1.0 and a coefficient of variation of 15%. The load model uncertainty is intended to allow for uncertainty in the calculated loads, for a given irregular wave input. It is effectively applied to both base shear and overturning moment, including both hydrodynamic and wind effects. The application to wind loads is incidental and of minor consequence, since they are relatively small. It should cover:

- the use of regular wave theory for a situation which is irregular in reality,
- any inaccuracy due to the chosen regular wave theory,
- inaccuracy due to the use of Morison's equation for the calculation of hydrodynamic loads,
- uncertainty in the selected values of drag and inertia coefficients, and marine growth.

The model uncertainty on the capacity is taken as a normal variable with a mean value of 1.0 and a coefficient of variation of 10%. These details are based on engineering judgment for the situation that the lateral pile capacity is governed by the lateral soil capacities along the pile and not by structural failure of the pile material. It is believed that a 10% coefficient of

variation in the model uncertainty of the lateral capacity of each of the 8 individual piles will be reflected in a coefficient of variation somewhat less than 10% in the model uncertainty factor for the global lateral capacity of the 8-pile foundation. Possible model uncertainties associated with the axial pile capacities and with the structural modelling, and of importance to the model uncertainty associated with the resulting global lateral capacity of the 8-pile foundation, are ignored. The ignored model uncertainty contributions from axial pile capacity and structural modelling are assumed to be balanced by the conservative model uncertainty contributions from the 8 lateral single pile capacities.

LOADS

A systematic set of hydrodynamic calculations with the WAJAC program (ref.[5]) is used to compute the hydrodynamic loading, for a full set of grid points specified by the selected values of the following parameters:

- water depths, 73.9 76.0, 78.0 m
- surface current speeds, 1.0, 1.1, 1.2 m/s
- bias factors on marine growth, 0.9, 1.0, 1.2 m/s
- regular wave periods, 9, 10, 12, 14 s
- regular wave heights, 8 10, 12, 14 16, 18 m.

Provision of response data for a full set of grid points permits use of a sequential splines type of response surface, as used in ref.[6]. The fit of the response surface to the data is checked and found to be most satisfactory. Figure 9 shows how this response surface is linked in to the reliability analysis by PROBAN.

Wind forces on the structure above the mean sea level are separately included in the analysis by a standard drag load formulation. The height of the line of action of the horizontal load is obtained for the sum of the wind load and the hydrodynamic load.

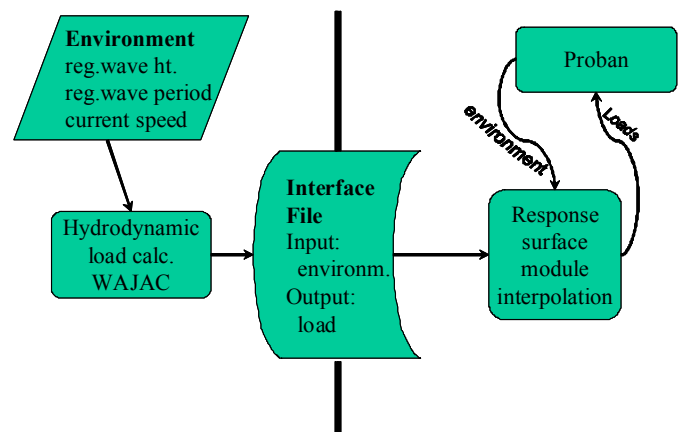


Figure 9 of response surface for hydrodynamic loads.

CAPACITY

Pile behaviour

The structural capacity of the system is strongly influenced by the soil surrounding the piles. Soil structure interaction was

modelled by spring elements in the structural analysis. A number of spring elements are distributed along the length of each pile, modelling both lateral and axial resistance. The nonlinear force / displacement characteristic of each spring element is calculated using the Gensod program [9]. Realisations of the random variables describing the soil properties provide input to this program.

The lateral resistance of the piles was modelled by means of cyclic p-y curves (lateral resistance – lateral displacement curves) representing the non-linear mobilisation of the soil resistance in the lateral direction. The curves were constructed based on the procedure first described by Matlock [10] and presently included as the recommended modelling procedure within the API framework of lateral bearing capacity for soft clay. These curves are generic, also with respect to the effect from cyclic loading as they specify a cut-off level at $U_{cy} = 0.72$, i.e 72% of the static resistance and a further degradation due to large displacements in the upper soils.

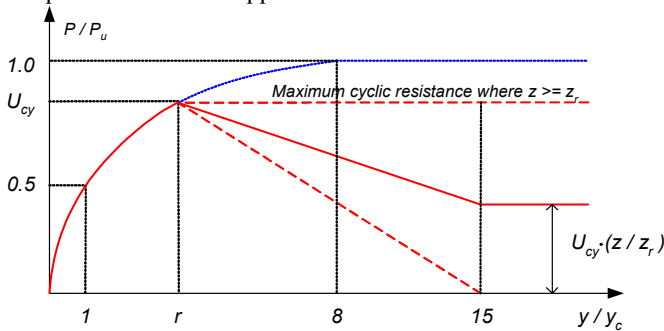


Figure 10 Construction of cyclic p-y curves

The axial resistance of the pile was modelled by means of t-z curves (pile skin friction – vertical displacement) and q-z curves (pile tip resistance – vertical displacement)

Generic resistance curves were generated using the recommended curves from API, the method presented by Kraft et al. [11]. The values of the skin friction was modified taking due account of the present excess pore pressure situation within the platform area.

Sensitivity to the axial capacity of the piles

A sensitivity analysis was conducted to check if an axial failure mode might occur instead of the lateral failure mode. For this purpose, the axial capacity was reduced to half the original design value, while the lateral capacity was retained at the original best estimate. Calculation of the system capacity showed that the failure still occurred in the same lateral failure mode, with no significant change in the overall capacity of the system.

Sensitivity to lateral soil resistance

A sensitivity study of the capacity to lateral soil resistance was made via the cyclic loading factor. It was found that a 10% change in the cyclic loading factor only leads to a 3% change in the capacity factor. The lateral soil resistance is closely related to the cyclic loading factor, as illustrated in Figure 10.

Response surface for capacity

A systematic set of pushover calculations with the USFOS program (ref.[1]) is used to compute the capacity factor on

base shear force, for various soil conditions. These results are arranged on a standard interface file for use in the polynomial type response surface module described in ref.[7]. Allowance for dependency of the capacity on the height of the line of action of the base shear force was originally included in the model, but subsequently dropped after sensitivity studies showed negligible effect in the present case. An example of the cut-plots used to check the fit of the response surface is shown in Figure 11. This shows how the fit of the response surface for capacity factor varies with a single input variable for the soil conditions, while the other input variables are held constant.

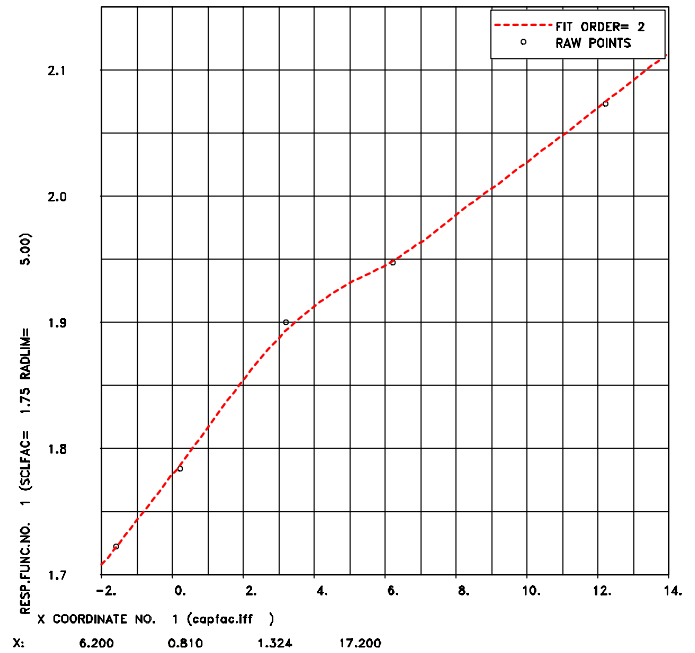


Figure 11 Cut-plot of response surface for capacity factor on base shear force against intercept of soil shear strength profile in kPa. Cut surface through $u_{cy} = 0.81$, $\epsilon_{s0} = 1.324$ %, $x_{pp} = 17.2$ kPa .

An overview of the response surface for capacity is shown in Figure 12. A typical detailed load distribution is applied in the collapse analyses. Variation of the wave period and wind load provides variation in the height of the line of action of the combined load for the sensitivity studies.

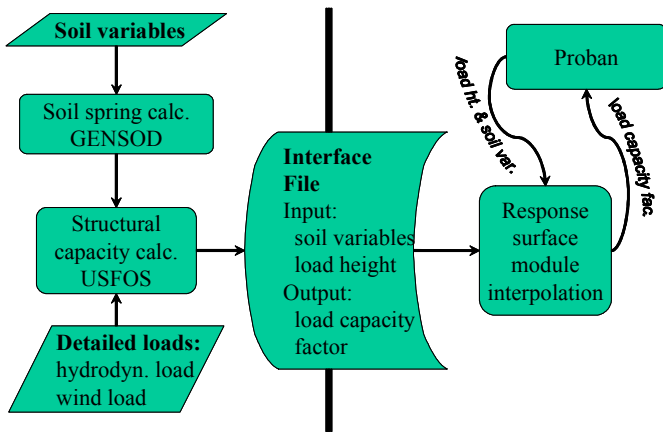


Figure 12 Overview of response surface for capacity.

RELIABILITY RESULTS

The structural reliability analysis is performed using the limit state formulation given above. The annual probability of structural failure is calculated to be 6×10^{-5} . The design point (most probable failure point) and importance factors for the basic stochastic variables are also calculated. The results show that the uncertainty in the environmental description is governing the results. This observation is not surprising since the distribution of the environmental variables has been established from a very limited data set (12 months measurements), and is therefore associated with large uncertainties. A considerably lower estimate for the failure probability would be expected if more environmental data were available.

The limit state formulation applied so far assumes that the wave crest will not impact on the deck structure. If the wave hits the deck then the load-effect will increase significantly. The quantification of impact loads on the deck is not straightforward and is associated with large uncertainties. A very much simplified and conservative approach is applied here to roughly quantify the effect of deck impacts; i.e. the conditional probability of failure given that the wave will not hit the deck is first calculated (result given above), and then the probability that the wave will hit the deck is added. This approach conservatively assumes that the structure will collapse if the wave crest hits the deck. The limit state for the event that the wave hits the deck can be formulated as:

$$g(x) = D - (\Psi_{*5} + C) \begin{cases} > 0, & \text{when the wave does NOT hit the deck} \\ = 0, & \text{when the wave touches the deck} \\ < 0, & \text{when the wave hits the deck} \end{cases} \quad (11)$$

where C is the crest height, Ψ_{*5} is the water depth and D is the lower deck level. The water depth is revised, because it is unconservative to assume a low tide in the context of deck impact. Instead, we model it as a uniformly distributed variable, with a mean value of 75.6m (mean water level 75.0m + storm surge 0.6m), and a range of ± 1 m for astronomical tide. The lower deck level is $D=88.4$ m above the sea bed. The crest height associated with the maximum wave height can be conservatively estimated as $0.6 \times H_{R*}$. The probability that the wave hits the deck is calculated to be about $4 \cdot 10^{-5}$.

The total annual failure probability is now approximated by summing the probability of failure for the two events: i.e. $6 \times 10^{-5} + 4 \times 10^{-5} = 1 \times 10^{-4}$

The following sensitivity studies have also been performed:

- water depth from 73m to 77m (base case water depth is 74.6 m)
- bias in marine growth thickness from 1.0 (base case) to 1.4
- regular wave periods from 11s to 13s (base case 12s)

The results from this study shows:

- The probability of failure increases somewhat with decreasing water depth e.g. for 73m the calculated failure is equal to $1. \times 10^{-4}$. The base case water depth of 74.6 has been chosen conservatively.
- Assuming exceptionally large increase in marine growth would be required to increase the probability of failure beyond $1. \times 10^{-4}$.
- The probability of failure increases weakly with increasing wave period. This corresponds to the weak increase in base shear force with increasing wave i.e. from $5. \times 10^{-5}$ (for 11s) to $7. \times 10^{-5}$ (for 13s).

The sensitivity results do not indicate any change in the estimated failure probability stated above.

CONCLUSION

Comprehensive reliability analysis was carried out for an ageing platform located in the South China Sea, in 75 m water depth. Gas seepage from the petroleum reservoir after installation of the platform has been taken into account in the modelling of the soil properties. Uncertainty in the environmental conditions, especially the wave height, dominates the computed probability of failure. This uncertainty is larger than usual, because the environmental model was stipulated to be based on measured data of only one year's duration. Year-to-year variability in the climate has additionally been taken into account, using hindcast data for a 20-year period. The uncertainty in the wave height distribution led to higher waves than originally expected, thus raising the possibility of deck impacts by the waves. Such deck impacts were not taken into account in the original analysis model. A rough, but conservative, allowance for the possible effect of deck impacts increased the estimated probability of failure to 7×10^{-5} . It is understood that this is less than the required target probability of failure. Hence, the analysis demonstrates that the platform still possesses adequate reliability with respect to collapse.

Sensitivity studies have been included, to check the effects of changes in input values for water depth, marine growth and wave period. Some sensitivity is found in the computed probability of failure with respect to these variables. However, the sensitivity results do not indicate any change in the conclusion stated above.

ACKNOWLEDGMENTS

The authors gratefully acknowledge permission to publish this paper from Petronas Research and Scientific Services and from Det Norske Veritas. Any opinions stated here are the responsibility of the authors and do not necessarily reflect the

views of these two companies. We would also like to acknowledge the cooperation of Knut Ronold, Arnfinn Reitan, Krishanth Krishnan and Hasmi Taib in the analysis described here.

REFERENCES

- [1] USFOS (1996); USFOS - A Computer Program for Progressive Collapse Analysis of Steel Offshore Structures, SINTEF Report no. STF71 F88039, Dated 1996-01-01.
- [2] Næss, A., (1985), "The joint crossing frequency of stochastic processes and its application to wave theory," J. Applied Ocean Research, Vol.7, No.1, 1985.
- [3] Sesam, (1996), "User's manual, PROBAN, General Purpose Probabilistic Analysis Program," DNV Software report no.92-7049, rev.no.1, Høvik.
- [4] Bitner-Gregersen, E.M, Haver,S., (1989), "Joint Long Term Description of Environmental Parameters for Structural Response Calculation," 2nd Int. Workshop on Wave Hindcasting & Forecasting, Vancouver.
- [5] Sesam, (2001), "User's Manual, WAJAC, Wave and Current Loads on Fixed Rigid Frame Structures," DNV Software report no. 92-7052, rev.no.2, Høvik.
- [6] Sigurdsson, G., Cramer, E., (1996), "Guideline for Offshore Structural Analysis – Examples for Jacket Platforms," Det Norske Veritas, report no. 95-3204, rev.no.01, Høvik.
- [7] Mathisen, J., (1993), "A Polynomial Response Surface Module for Use in Structural Reliability Computations," Det Norske Veritas, report no.93-2030, Høvik.
- [8] Ladd, C.C., et al, (1977), "Stress Deformation and Strength Characteristics," Proc. 9th Int. Conf. on Soil Mech., 2, Tokyo, Japan, pp 421-494.
- [9] SESAM, (1992), "SPICE, Structure/Pile/Soil Interaction Analysis, User's Manual," DNV Software report no. 90-7016, rev.no.1, Høvik.
- [10] Matlock, H. (1970) "Correlation for Design of Laterally Loaded Piles in Soft Clay," OCT Paper 1204, Vol.1 pp 557-588.
- [11] Kraft, L.M., Ray R.P. and Kagawa, T. (1981) "Theoretical t-z curves", American Society of Civil Engineers, Proceeding, Vol. 107, No. GT11, November 1981 pp. 1543 – 1561.